ETH zürich

ETH Library

Minimum transmissivity and optimal well spacing and flow rate for high-temperature aquifer thermal energy storage

Journal Article

Author(s):
Birdsell, Daniel T.; Adams, Benjamin; Saar, Martin O.

Publication date:
2021-05

Permanent link:
https://doi.org/10.3929/ethz-b-000473035

Rights / license:
Creative Commons Attribution 4.0 International

Originally published in:
Applied Energy 289, https://doi.org/10.1016/j.apenergy.2021.116658

This page was generated automatically upon download from the ETH Zurich Research Collection.
For more information, please consult the Terms of use.

Applied Energy 289 (2021) 116658

Contents lists available at ScienceDirect

Applied Energy

journal homepage: www.elsevier.com/locate/apenergy

Minimum transmissivity and optimal well spacing and flow rate for high-temperature aquifer thermal energy storage

Daniel T. Birdsell [a,*], Benjamin M. Adams [a], Martin O. Saar [a,b]

[a] Geothermal Energy and Geofluids Group, Department of Earth Sciences, ETH Zürich, Sonneggstrasse 5, 8092 Zürich, Switzerland
[b] Department of Earth and Environmental Sciences, University of Minnesota, 116 Church Street SE, Minneapolis, MN, 55455, USA

ARTICLE INFO

Keywords:
High-temperature aquifer thermal energy storage
HT-ATES
Heat storage
Reservoir engineering
Levelized cost of heat
Geothermal energy

ABSTRACT

Aquifer thermal energy storage (ATES) is a time-shifting thermal energy storage technology where waste heat is stored in an aquifer for weeks or months until it may be used at the surface. It can reduce carbon emissions and HVAC costs. Low-temperature (< 25 °C) aquifer thermal energy storage (LT-ATES) is already widely-deployed in central and northern Europe, and there is renewed interest in high-temperature (> 50 °C) aquifer thermal energy storage (HT-ATES). However, it is unclear if LT-ATES guidelines for well spacing, reservoir depth, and transmissivity will apply to HT-ATES. We develop a thermo-hydro-mechanical-economic (THM$) analytical framework to balance three reservoir-engineering and economic constraints for an HT-ATES doublet connected to a district heating network. We find the optimal well spacing and flow rate are defined by the "reservoir constraints" at shallow depth and low permeability and are defined by the "economic constraints" at great depth and high permeability. We find the optimal well spacing is 1.8 times the thermal radius. We find that the levelized cost of heat is minimized at an intermediate depth. The minimum economically-viable transmissivity (MEVT) is the transmissivity below which HT-ATES is sure to be economically unattractive. We find the MEVT is relatively insensitive to depth, reservoir thickness, and faulting regime. Therefore, it can be approximated as $5 \cdot 10^{-13}$ m^3. The MEVT is useful for HT-ATES pre-assessment and can facilitate global estimates of HT-ATES potential.

1. Introduction

The heating and cooling of buildings comprise roughly half of the world's final total energy consumption and are driven primarily by fossil fuels, resulting in substantial emissions of greenhouse gases [1], NO_x, and SO_x [2]. Thermal energy storage may reduce greenhouse gas emissions in two ways. First, in a system where heating and electricity networks are integrated, thermal energy storage can facilitate demand side management, which may lead to augmented use of variable renewable electricity sources like wind and solar [3]. Second, seasonal thermal energy storage can shift the thermal energy supply to times of thermal energy demand [1], thereby potentially reducing the amount of energy required and carbon emitted. Seasonal thermal storage can be located in underground pits, tanks, mines, caverns, and aquifers, where large amounts of sensible heat can be stored with high efficiency. Aquifer thermal energy storage (ATES) has the largest storage capacity among these options [1].

Typical ATES operations involve two stages: a summer stage and a winter stage. In the summer stage, water is extracted from a "cold" well, heated with waste heat that cannot be otherwise utilized, and then re-injected into a "hot" well. In the winter stage, this process is reversed, and water is extracted from the hot well, used for heating, and is injected into the cold well at a lower temperature. As opposed to direct-use geothermal heating, ATES treats the reservoir as a storage tank and not an energy source. ATES's heat is typically used in large commercial or industrial buildings, city-wide district heating networks (DHNs), or greenhouses.

There are two classes of aquifer thermal energy storage: low-temperature ATES and high-temperature ATES. Low-temperature ATES (LT-ATES) typically stores temperatures less than 25 °C. LT-ATES is widely implemented and generally considered technically and economically successful, with thousands of installations worldwide and payback periods between 2–10 years [1]. In addition to heating, many LT-ATES systems are also used for cooling in the summer. This cooling is possible because the cold well has a sufficiently low temperature to accept heat. High-temperature ATES (HT-ATES) typically stores temperatures greater than 50 °C. In contrast to LT-ATES, HT-ATES is only used for heating because the temperature at the cold well is too high for cooling purposes [4].

* Corresponding author.
E-mail address: danielbi@ethz.ch (D.T. Birdsell).

https://doi.org/10.1016/j.apenergy.2021.116658
Received 3 November 2020; Received in revised form 10 February 2021; Accepted 11 February 2021
Available online 26 February 2021
0306-2619/© 2021 The Authors. Published by Elsevier Ltd. This is an open access article under the CC BY license (http://creativecommons.org/licenses/by/4.0/).

Nomenclature

Acronyms

ATES	Aquifer thermal energy storage
COP	Coefficient of performance
DHN	District heating network
GETEM	Geothermal electricity technology evaluation model
HF	Hydraulic fracturing
HT-ATES	High-temperature aquifer thermal energy storage
LCOH	Levelized cost of heat
LT-ATES	Low-temperature aquifer thermal energy storage
MEVP	Minimum economically-viable permeability
MEVT	Minimum economically-viable transmissivity
NRGF	Natural regional groundwater flow
THM$	Thermo-hydro-mechanical-economic

Superscripts and Subscripts

$*$	Optimal value
$econ$	Related to the "economic constraints" and the "economic-constrained regime"
I, II, III	Related to the first, second, and third constraint, respectively
res	Related to the "reservoir constraints" and the "reservoir-constrained regime"
th	Thermal

Variables and Parameters

α_{II}	Ratio of the minimum principal stress to the lithostatic stress
α_I	Fraction of reservoir volume available for heat extraction
ΔL	Assumed distance for temperature gradient approximation
ΔP_{inj}	Change in pressure at injection well
ΔT	Temperature difference between the extracted hot fluid and the injected cold fluid during the heat extraction stage
Δt	The duration of heat extraction
η	Thermal efficiency
γ	The ratio of HT-ATES's heating cost to the cost of electricity
λ_{eff}	Effective thermal conductivity
μ	Dynamic fluid viscosity
ϕ	Porosity
ρ_f	Fluid density
ρ_r	Rock density
A	Interfacial area for heat-loss calculation
b	Reservoir thickness
c	Price of electricity
C_1	Conversion constant [kWh/J]
C_{cap}	Capital cost
C_{op}	Annual operating cost
$C_{p,f}$	Fluid heat capacity
$C_{p,r}$	Rock heat capacity
CRF	Capital recovery factor
D	Well diameter
d	Reservoir depth
$d^*_{constraints}$	The depth where all three constraints are equal
d^*_{kmin}	The depth where the MEVP is minimized
d^*_{LCOH}	The depth where the LCOH is minimized
E	Total amount of heat extracted during the "Heat Extraction" stage
k	Permeability
L	Well spacing
m	Mass flow rate into injection well and out of production well
n	Project lifetime
Q	Annual heat recovered
Q_c	Conductive heat loss from the reservoir
r	Discount rate
R_{th}	Thermal radius
T_{CV}	Temperature in the heated control volume at the end of the resting stage
T_{DH}	District heat return temperature
T_G	Background geothermal temperature
T_{WH}	Summertime waste heat temperature
V_{HL}	The reservoir volume from which heat is lost
V_{res}	Reservoir volume
W	Work done by the pump during the extraction stage

Previous studies recommend that well spacing should range from just over one [5] to more than three [6] thermal radii for LT-ATES. The thermal radius is the radial extent of a thermal plume, assuming horizontal, cylindrical flow away from an injection well in a homogeneous media [7]. Early work considered a doublet (i.e., a well pair) and showed that thermal breakthrough could significantly reduce the thermal efficiency [5]. More recently, work has considered LT-ATES planning at a city-wide scale, where many wells compete for limited subsurface space [7–9]. For cities with a congested subsurface, there is a tradeoff between optimizing an individual well's thermal efficiency and maximizing the total amount of heat that can be stored underground by installing LT-ATES wells more densely. Therefore, it can make economic sense to reduce the well spacing somewhat to provide more heat [7,9]. In considering non-homogeneous reservoirs, Sommer et al. [10] found that heterogeneity in the permeability field increases the thermal diffusivity. Therefore, the optimal well spacing also depends on the degree of heterogeneity in the reservoir [10].

There are also recommendations on depth and transmissivity for LT-ATES. Reservoir transmissivity is the product of permeability and reservoir thickness. The permeability should be at least $3 \cdot 10^{-12}$ m^2 and is more typically in the range of $1 \cdot 10^{-11}$–$5 \cdot 10^{-11}$ m^2 [11,12]. The thickness should be at least 2 m and is more typically 20–50 m [11,12]. Therefore, the minimum transmissivity is on the order of 10^{-11} m^3, with more typical values being one to two orders of magnitude higher. The reservoir depth is typically 30–100 m, with an upper limit of 300 m [11]. Snijders and Drijver [11] suggest the upper limit on depth is due to economic feasibility.

HT-ATES has several potential advantages over LT-ATES. Firstly, higher temperature fluid has a higher energy density, and therefore each cubic meter has a higher economic value. Secondly, operating at higher temperatures could negate the need for a heat pump to upgrade the temperature before the fluid enters a DHN, thereby reducing complexity and capital costs [4]. Finally, HT-ATES can store large amounts of heat (up to 100 GW$_{th}$h/yr [13]), and typically targets deeper reservoirs than LT-ATES [4,13]. Therefore, HT-ATES could

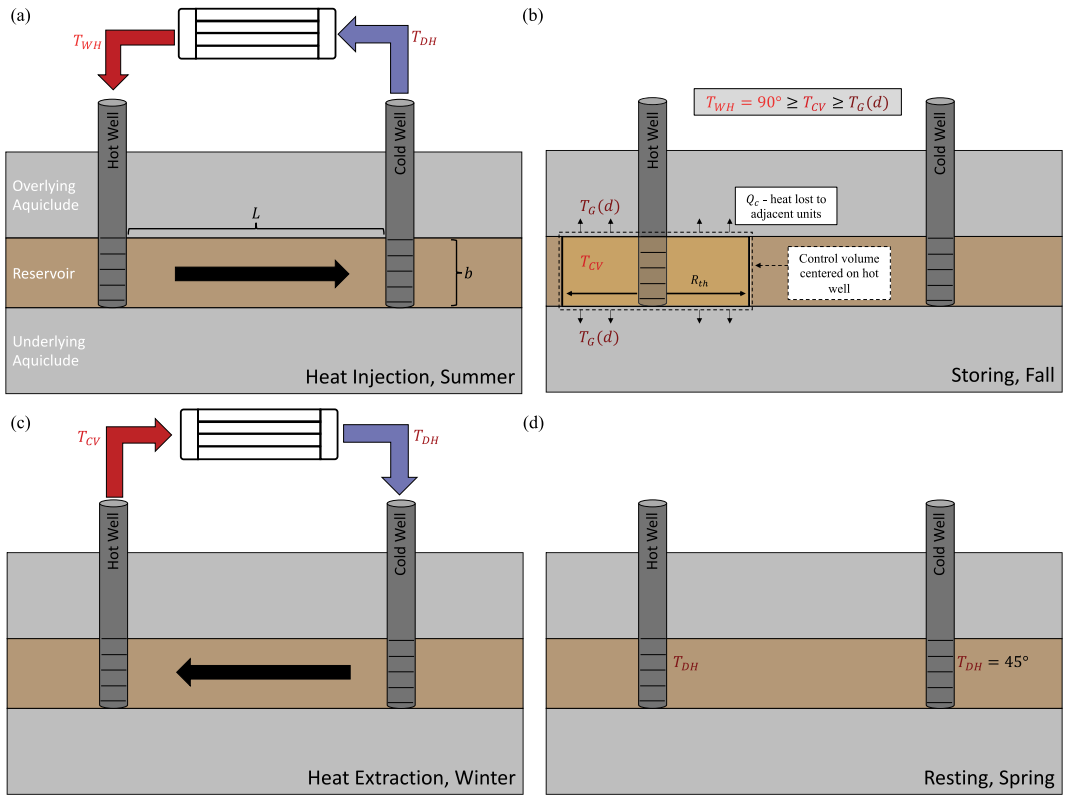

Fig. 1. Conceptual model of a HT-ATES doublet for (a) heat injection, (b) storing, (c) heat extraction, and (d) resting stages. Bold arrows indicate the direction of flow, when relevant.

potentially relieve the congestion due to LT-ATES in the shallow subsurface under some cities by: (a) expanding the total thermal storage available and (b) targeting depths that do not compete with LT-ATES.

While the HT-ATES literature is more limited than the LT-ATES literature, it offers some insight into favorable permeability, reservoir thickness, and well spacing. Firstly, excessive permeability can result in significant advective heat loss due to thermally-driven buoyancy [14]. But on the other hand, if the permeability is too small, then it is difficult to inject and extract meaningful quantities of fluid and heat [15]. Therefore, it is likely that some intermediate permeability is favorable. Secondly, the reservoir thickness affects the thermal efficiency by altering the shape of the thermal stock and therefore the heat loss [15,16]. Finally, thermo-hydraulic numerical modeling with natural regional groundwater flow (NRGF) performed by Gao et al. [16] suggests that the well spacing should be 3.5 thermal radii.

Despite previous studies, guidelines for transmissivity, well spacing, and depth are not definitively established for HT-ATES. For one thing, there is no consensus on the suggested permeability and reservoir thickness. The value of permeability that is too large (i.e., associated with buoyancy-driven advective heat loss) is generally believed to be $\approx 5 \cdot 10^{-13}$ m^2 [14,17], but it could be one to two orders of magnitude higher [16]. The value of permeability that is too low (i.e., that limits fluid flow into and out of the reservoir) is also uncertain. It depends not only on thermal efficiency but also on avoiding hydro-mechanical problems that occur with excessive pore pressure [18] and on the levelized cost of heat (LCOH) that is deemed economically acceptable. For reservoir thickness, the Résonance [15] study suggests that thin reservoirs are preferred, while the Gao et al. [16] study indicates that medium-thickness reservoirs are favorable. As a second point, most of the HT-ATES studies cited in the previous paragraph utilize parametric hydro-thermal numerical modeling. While this approach plays an important role in defining guidelines, it also has potential limitations. Firstly, it is hard to guarantee that guidelines taken from these studies apply for all possible combinations of subsurface conditions. For example, the Gao et al. [16] recommendation for well spacing was found in the presence of NRGF, which encourages earlier thermal breakthrough than an initially-static reservoir. Secondly, while hydro-thermal models do an excellent job of constraining an HT-ATES system's thermal efficiency, there are hydro-mechanical and economic aspects for which hydro-thermal models cannot provide insight.

In this paper, we model an HT-ATES doublet with varying reservoir transmissivity and depth. We find: (a) the flow rate, well spacing, and depth that is technically and economically attractive for HT-ATES systems, and (b) the minimum economically-viable transmissivity (MEVT) of an HT-ATES reservoir, which is useful to pre-screen potential reservoirs. In Section 2, we develop a thermo-hydro-mechanical-economic (THM$) analytical framework to evaluate HT-ATES constraints related to reservoir engineering and economics. To our knowledge, this is a novel approach; previous studies have not coupled thermo-hydro-mechanical reservoir engineering and economics to create guidelines for HT-ATES. In Section 3, we apply the THM$ framework to understand the optimal flow rate, well spacing, and depth. We also present LCOH calculations, which allow us to find the MEVT. Sections 4 and 5 provide practical implications, discuss limitations of our approach, and conclude with main takeaways.

2. Methods

Our THM$ methodology considers a generic HT-ATES doublet, which is shown in Fig. 1 and discussed in more detail throughout Section 2. The conceptual model includes four stages: (a) heat injection, (b) storing, (c) heat extraction, and (d) resting, which each last one quarter of a year and correspond roughly to summer, fall, winter, and spring, respectively. No water is injected or extracted through the wells in the storing or resting stages. Our THM$ framework can be expressed analytically, but it uses Python for variable passing, interpolation, and

to solve implicit equations. This code is published as an open-source companion to this manuscript [19].

Fig. 2 shows a block-diagram overview of the THM$ calculations. First, all the reservoir and economic parameters must be specified. Second, the well spacing and flow rate are calculated in two ways: (a) from the reservoir constraints and (b) from the economic constraints (defined in Section 2.3). Third, the optimal well spacing and flow rate are calculated as the minimum of the two well spacing and flow rate values, respectively. Finally, additional performance metrics such as the LCOH, thermal efficiency, heat loss, reservoir temperature, and MEVT are calculated.

While the summary of the THM$ methodology in Fig. 2 is simple, more detail must be provided in the following subsections. Sections 2.1 and 2.2 provide governing equations for a well doublet and the three reservoir-engineering and economic constraints that the THM$ approach considers. In Section 2.3, we show how to calculate the optimal flow rate and well spacing. In Section 2.4, we give more details about the equations used to describe heat loss and heat recovery, which are important to evaluate the economic attractiveness and other performance metrics of a HT-ATES system. In Section 2.5, we define the MEVT and explain the conservative assumptions behind it.

2.1. Overview equations for a well doublet

For a doublet system, the change in pressure at the injection well (i.e., the interface between the well screen and the porous media) is approximated by integrating the Darcy equation for fluid flow in porous media [20]:

$$\Delta P_{inj} = \frac{m\mu}{2\pi\rho_f(kb)} \ln\left(\frac{L}{D}\right) \tag{1}$$

where m is the mass flow rate into the injection well and out of the production well, μ is the dynamic fluid viscosity, ρ_f is the fluid density, k is the permeability, b is the reservoir thickness, L is the well spacing, and D is the well diameter. Eq. (1) assumes a flat, homogeneous, isotropic reservoir with a uniform initial hydraulic head, perfect aquicludes above and below, a fully-penetrating well, negligible changes in fluid density, and a system that has approached steady state. While simple, Schaetzle et al. [20] note that this solution gives relatively reliable results, and we confirmed in offline calculations that the error is typically less than 20% for the parameter ranges explored in this paper when compared to a more complex solution [21]. Since we are interested in a first-order, analytical analysis, we elect to use Eq. (1), due to its relatively simple form and relatively small error. Note that kb is the reservoir transmissivity with units of L^3, and we keep these terms grouped in parenthesis throughout many equations in this paper to highlight the importance of transmissivity. The pressure change at the production well has the same magnitude but the opposite sign, so the total pressure difference between the two wells is $2\Delta P_{inj}$. By using Eq. (1), we are neglecting pressure losses very near the well (i.e., the skin factor) and within the wells. This is a reasonable approximation, since these tend to be smaller than pressure losses within the reservoir [22].

The COP is a measure of the useful heat extracted from the reservoir to the pumping work required to store and extract that heat. During the heat extraction stage, the total amount of heat extracted is: $E = mC_{p,f}\Delta T\Delta t$ where $C_{p,f}$ is the water's heat capacity, ΔT is the temperature difference between the extracted hot fluid and the injected cold fluid during the heat extraction stage, and Δt is the duration of the heat extraction. Assuming perfectly-efficient pumps, the work during the extraction stage is: $W = 2m\Delta P_{inj}\Delta t/\rho_f$. Therefore, using Eq. (1), the COP during heat extraction can be expressed as:

$$COP = \frac{E}{W} = \frac{mC_{p,f}\Delta T\Delta t}{2m\Delta P_{inj}\Delta t/\rho_f} = \frac{\rho_f^2 C_{p,f}\Delta T\pi(kb)}{m\mu\ln(L/D)} \tag{2}$$

The parameters for our base-case scenario are shown in Table 1. If parameters are changed in parts of the Results (Section 3), they are explicitly noted.

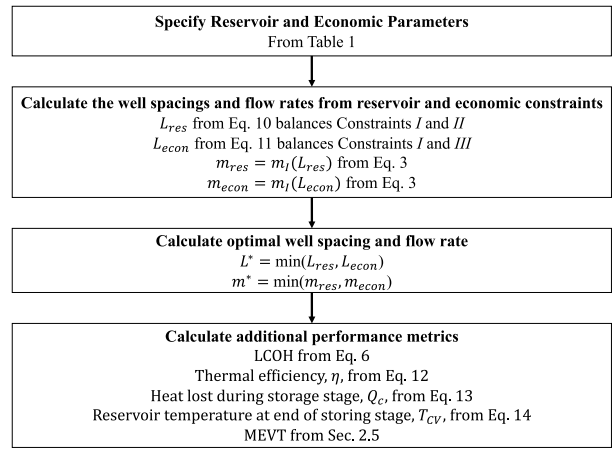

Fig. 2. Block diagram for the THM$ calculations.

Table 1
Parameters for base-case scenario.

Parameter description	Variable	Value	Unit
Reservoir thickness	b	20	m
Permeability	k	10^{-13}	m^2
Fluid heat capacity	$C_{p,f}$	4186	J/kg/°C
Rock heat capacity	$C_{p,r}$	850	J/kg/°C
Fluid density	ρ_f	1000	kg/m^3
Rock density	ρ_r	2500	kg/m^3
DHN return temperature	T_{DH}	45	°C
Waste heat temperature	T_{WH}	90	°C
Well hydraulic diameter	D	0.261	m
Fluid viscosity	μ	$5 \cdot 10^{-4}$	Pa-s
Porosity	ϕ	0.15	–
Stage duration	Δt	1/4	yr
Reservoir depth	d	575	m
Constraint I parameter	α_I	1	–
Constraint II parameter	α_{II}	1	–
Effective thermal conductivity	λ_{eff}	2.64	W/m/°C
Heat conduction length parameter	ΔL	5	m
Cost of electricity (Section 2.4)	c	0.10	$/kWh
ATES Lifetime	n	25	yr
Discount rate	r	0.03	–
Convert Joules to kWh	C_1	$2.8 \cdot 10^{-7}$	kWh/J

2.2. Three constraints

In this paper, we analyze and balance three constraints that apply to HT-ATES systems:

- Constraint I defines a maximum flow rate so that the reservoir's thermal capacity is not over-utilized.
- Constraint II defines a maximum flow rate so that the reservoir pressure does not lead to hydraulic fracturing (HF).
- Constraint III defines the flow rate that minimizes the levelized cost of heat (LCOH). It does not make sense to pump at flow rates above the flow rate that minimizes LCOH, so Constraint III defines a "maximum" flow rate in the same way as Constraints I and II.

Constraint I is related to hydro-thermal reservoir engineering, Constraint II is related to hydro-mechanical reservoir engineering, and Constraint III is related to economics (and hydro-thermal reservoir engineering to a lesser degree). These three constraints form the backbone of our THM$ approach. This is not a fully-coupled approach, which would require numerical simulation. Instead, we take an analytical approach which reduces complexity so that it is possible to consider insights from the full set of THM$ constraints with short computational times.

Constraint I defines the maximum flow rate for which a reservoir will be able to store heat effectively. The amount of heat that a reservoir

can hold is: $(\rho_f C_{p,f}\phi + \rho_r C_{p,r}(1-\phi))V_{res}(T_{WH} - T_{DH})$, where ϕ is the porosity, ρ_r is the rock density, $C_{p,r}$ is the rock's heat capacity, V_{res} is the useful reservoir volume, and $T_{WH} - T_{DH}$ is the temperature difference between the injected and extracted fluid during the heat injection stage (see Fig. 1 and Section 2.4 for more detail). We assume that the useful reservoir volume is $V_{res} = (\alpha_I L)^2 b$, where α_I is the fraction of the reservoir volume available for heat extraction and has an assumed value of one. The amount of energy injected during the heat injection stage is $mC_{p,w}\Delta t(T_{WH} - T_{DH})$. By equating the amount of heat a reservoir can hold with the amount injected, we find a maximum flow rate, which is a function of, among other parameters, the reservoir thickness and well spacing:

$$m_I \leq \frac{(\phi\rho_f C_{p,f} + (1-\phi)\rho_r C_{p,r})((\alpha_I L)^2 b)}{C_{p,f}\Delta t} \tag{3}$$

If the flow rate exceeds m_I, additional heat will not be stored effectively, and pumping electricity is wasted.

Constraint II defines the maximum flow rate that can be supported without HF the reservoir. HF occurs when the pore pressure exceeds the minimum principal stress plus the tensile strength of the rock. We neglect tensile strength and assume a form for the minimum principal stress as: $\alpha_{II}\rho_r g d$ where α_{II} is the ratio of the minimum principal stress to the lithostatic stress and d is the reservoir depth. For reverse faulting regimes, $\alpha_{II} = 1$ according to Anderson's faulting classifications, because the minimum principal stress is the lithostatic stress [23]. Our base-case scenario uses $\alpha_{II} = 1$, which allows higher flow rates than if $\alpha_{II} < 1$, in normal and strike-slip faulting regimes. Assuming that the reservoir pore pressure is hydrostatic initially, and utilizing Eq. (1), we write the mass flow rate to avoid hydraulic fracturing.

$$m_{II} \leq \frac{2\pi\rho_f(kb)}{\mu\ln(L/D)}\left((\alpha_{II}\rho_r - \rho_f)gd\right) \tag{4}$$

By combining Eq. (2) with Eq. (4), we can also express Constraint II in terms of COP.

$$COP_{II} \geq \frac{\rho_f C_{p,f}\Delta T}{2(\alpha_{II}\rho_r - \rho_f)gd} \tag{5}$$

Constraint III defines the flow rate that minimizes the LCOH. We calculate LCOH according to:

$$LCOH = \frac{C_{cap}\cdot CRF + C_{op}}{Q} = \frac{C_{cap}\cdot CRF}{mC_{p,f}\Delta T\Delta t C_1} + \frac{2\ mc\mu\ln(L/D)}{\pi\rho_f^2(kb)C_{p,f}\Delta T} \tag{6}$$

where C_{cap} is the capital cost, CRF is the capital recovery factor, C_{op} is the annual operating cost, and Q is the annual heat recovered. The operating cost is the pumping work multiplied by the cost of electricity. Using Eqs. (1) and (2), it can be expressed as: $C_{op} = 2\ m^2\Delta t C_1 c\mu\ln(L/D)/\pi\rho_f^2(kb)$, where $C_1 = 2.8\cdot 10^{-7}$ kWh/J is a constant to convert units, and c is the price of electricity. The annual heat recovered in kWh is: $Q = mC_{p,f}\Delta T\Delta t C_1$. Maintenance costs are assumed to be negligible. The capital costs occur at the beginning of the project and are assumed to be twice the cost of the wells, which agrees with costs for the ATES system in Rostock, Germany [12]. The well cost is taken from the Geothermal Electricity Technology Evaluation Model (GETEM) for a borehole with a 31 cm diameter and is expressed in terms of 2019 US dollars [24]. Multiplication of capital cost with the capital recovery factor turns the capital cost into an equivalent annualized cost. CRF is defined as:

$$CRF = \frac{r(1+r)^n}{(1+r)^n - 1} \tag{7}$$

where r is the discount rate and n is the lifetime of the project. We assume a discount rate of 3%, a twenty-five year project lifetime, and an electricity cost of \$0.10/kWh.

The flow rate that results in the minimum LCOH can be found by taking the derivative of Eq. (6) with respect to m and setting to zero.

$$\begin{aligned}\frac{d(LCOH)}{d\ m} &= \frac{-C_{cap}\cdot CRF}{mQ} + \frac{C_{op}}{mQ}\\ &= \frac{-C_{cap}\cdot CRF}{m^2 C_{p,f}\Delta T\Delta t C_1} + \frac{2c\mu\ln(L/D)}{C_{p,f}\Delta T\rho_f^2\pi(kb)} = 0\end{aligned} \tag{8}$$

Solving the previous equation for m gives the flow rate that minimizes LCOH:

$$m_{III} = \left(\frac{C_{cap}\cdot CRF\rho_f^2\pi(kb)}{2C_1 c\Delta t\mu\ln(L/D)}\right)^{1/2} \tag{9}$$

If the flow rate is greater than the equation above, then the pumping cost is large, which increases the LCOH. If the flow rate is less than the equation above, then the LCOH can be decreased by increasing the flow rate, thereby recovering more heat each year. Interestingly, it can be seen from Eq. (8) that the LCOH is minimized when the annual operating cost equals the equivalent annualized capital cost.

2.3. Optimal flow rate and well spacing

The three constraints from the previous section can be further combined into the "reservoir constraints" and the "economic constraints". The reservoir constraints include Constraints I and II. They apply at shallow depth or low permeability, and we call this part of the parameter space the "reservoir-constrained regime". The economic constraints include Constraints I and III. They apply at great depth or high permeability, and we call this part of the parameter space the "economic-constrained regime".

The optimal well spacing and flow rate have different relationships, depending if the HT-ATES reservoir exists in the reservoir-constrained regime or the economic-constrained regime.

- *Reservoir-constrained regime:* In the reservoir-constrained regime, the well spacing and flow rate are denoted L_{res} and m_{res}, respectively. m_{res} represents the maximum flow rate that the reservoir can support, without HF or injecting more heat than the reservoir can hold. By equating m_I (Eq. (3)) with m_{II} (Eq. (4)), we find an implicit expression for the well spacing:

$$\begin{aligned}&(L_{res})^2\cdot\ln(L_{res}/D) - \frac{2\pi\rho_f k}{\mu}\left((\alpha_{II}\rho_r - \rho_f)gd\right)\\ &\times\frac{C_{p,w}\Delta t}{(\phi\rho_f C_{p,f} + (1-\phi)\rho_r C_{p,r})} = 0\end{aligned} \tag{10}$$

- *Economic-constrained regime:* In the economic-constrained regime, the well spacing and flow rate are denoted L_{econ} and m_{econ}, respectively. By equating m_I (Eq. (3)) with m_{III} (Eq. (9)), we find an implicit expression for L_{econ}:

$$\begin{aligned}&\left(\frac{C_{cap}\cdot CRF\rho_f^2\pi(kb)}{2C_1 c\Delta t\mu\ln(L_{econ}/D)}\right)^{1/2}\\ &-\frac{(\phi\rho_f C_{p,f} + (1-\phi)\rho_r C_{p,r})((\alpha_I L_{econ})^2 b)}{C_{p,f}\Delta t} = 0\end{aligned} \tag{11}$$

The optimal well spacing and flow rate can be determined in several steps. First, the well spacing from the reservoir and economic constraints (L_{res} and L_{econ}, respectively) are calculated using Eqs. (10) and (11). Then, the flow rates from the reservoir and economic constraints (m_{res} and m_{econ}) are calculated by using L_{res} and L_{econ}, respectively, in Eq. (3). Finally, the optimal flow rate is set as the minimum of m_{res} and m_{econ}, which ensures that the three constraints from Section 2.2 are not violated. Similarly, the optimal well spacing is also set to the minimum of L_{res} and L_{econ}.

2.4. Heat loss and recovery

As the depth and geothermal temperature increase, we expect less heat loss, greater thermal efficiency, and more overall heat production, if all else is held constant. This section develops a conceptual and mathematical model of heat loss and recovery that honors these aforementioned trends. Our conceptual model was introduced at the beginning of Section 2 and is illustrated in Fig. 1, but we describe it in more detail here. During the heat injection stage, fluid is injected

into the hot well at the temperature supplied from the summertime waste heat source, T_{WH}. Simultaneously, fluid is produced from the cold well at a temperature of T_{DH}, the wintertime district heat return temperature. During the storing stage, we assume that heat is irrecoverably lost from the reservoir to the aquicludes. We assume this heat loss occurs from a cylindrically-shaped control volume with thermal radius R_{th} and thickness b, and we define the average temperature at the end of the storing stage in the control volume as T_{CV}. During the heat extraction stage, the remaining thermal energy in the control volume is recovered (to a cut off temperature of T_{DH}), such that $\Delta T = T_{CV} - T_{DH}$ in Eqs. (2), (5), and (6). For simplicity, we assume that the DHN is perfectly efficient, so that all the heat at $T > T_{DH}$ is useful to the DHN. We do not consider the use of heat pumps, which could bring lower-temperature fluid up to a useful temperature for the DHN. In the resting stage, we assume that the water near the hot and cold wells remains at T_{DH}, which is important for the start of the next heat injection stage. We approximate the thermal efficiency of the HT-ATES system as:

$$\eta = \frac{mC_{p,f}\Delta t(T_{CV} - T_{DH})}{mC_{p,f}\Delta t(T_{WH} - T_{DH})} = \frac{(T_{CV} - T_{DH})}{(T_{WH} - T_{DH})} \tag{12}$$

In Eq. (12), $T_{DH} = 45$ °C and $T_{WH} = 90$ °C are assumed from surface constraints, which seem reasonable for HT-ATES and fourth-generation DHNs [25,26]. To solve for T_{CV}, we assume that heat losses are purely conductive to the overlying and underlying aquicludes. Neglecting buoyancy-driven advective heat loss appears to be justified for $k < 5{\cdot}10^{-13}$ m^2 [14,17]. We assume that heat losses can be described by:

$$Q_c = -\lambda_{eff} A \nabla T \approx -\lambda_{eff} A \frac{T_{CV}(t) - T_G}{\Delta L} \tag{13}$$

where λ_{eff} is the effective thermal conductivity of the rock/water mixture, A is the interfacial area between the hot control volume and the overlying and underlying rock, $T_{CV}(t)$ is the temperature in the control volume as a function of time (and is distinct from T_{CV} which is the temperature at the end of the resting stage), T_G is the background geothermal temperature, and ΔL is an assumed distance over which the temperature gradient is approximated. The geothermal temperature is a function of depth and assumes a surface temperature of 10 °C and a geothermal gradient of 30 °C/km. ΔL is assumed to be 5 m, because previous modeling work has shown that the temperature fronts remain fairly sharp [14]. The use of $\Delta L = 5$ m is further justified because it results in thermal efficiencies that are within the range of numerical models of HT-ATES for similar reservoir properties and cut-off temperatures [14,15]. By accounting for the energy accumulation and heat-loss terms, we can write an ODE for T_{CV} and solve for the average temperature within the control volume as a function of time. At the end of the resting stage, the temperature is:

$$T_{CV} = (T_{WH} - T_G)\exp\left(\frac{-C_3 \Delta t}{C_2}\right) + T_G \tag{14}$$

where $C_2 = ((1-\phi)\rho_r C_{p,r} + \phi\rho_f C_{p,f})V_{HL}$, $C_3 = \lambda_{eff} A/\Delta L$, and V_{HL} is the reservoir volume over which heat loss occurs. Note that we used the initial condition $T_{CV}(t=0) = T_{DH}$ to arrive at the solution above. The reservoir volume over which heat loss occurs can be approximated from either the well spacing or the thermal radius as $V_{HL} = (\alpha_{II} L)^2 b$ or $V_{HL} = \pi R_{th}^2 b$, respectively. Similarly, the interfacial area between the thermally-affected reservoir and the cold, overlying and underlying units can also be expressed in terms of the well spacing or the thermal radius as $A = 2L^2$ or $A = 2\pi R_{th}^2$, respectively. It is not clear in general if the well-spacing or the thermal-radius provide better approximations of the heat loss volume and interfacial area. However, the thermal radius approximation does have one advantage: it scales the size of the thermally-effected region with the flow rate, and we therefore use $V_{HL} = \pi R_{th}^2 b$ and $A = 2\pi R_{th}^2$.

2.5. Minimum economically-viable transmissivity

Our goal is to find the minimum economically-viable transmissivity (MEVT) (and a related measure, the minimum economically-viable permeability (MEVP)), which is the transmissivity (and permeability) below which HT-ATES is sure to be economically unattractive. The MEVT can provide a useful lower bound on reservoir transmissivity, allowing one to quickly and easily eliminate potential reservoirs that have a transmissivity below the MEVT. We take two steps to ensure that the MEVT truly is a lower bound on economic viability, so that reservoirs are not unduly eliminated from consideration. Firstly, we define the MEVT as the transmissivity that results in HT-ATES LCOH being equal to the cost of an expensive heating alternative, namely electrical resistant heating. If we had chosen a cheaper heating alternative (e.g., a natural gas boiler), then the transmissivity would need to be larger to have cost parity. Secondly, we make many conservative assumptions in our HT-ATES model that favor lower LCOH. These assumptions include:

1. We neglect costs related to the construction and maintenance of a DHN, which are necessary for most large-scale HT-ATES.
2. We also neglect the maintenance costs of the HT-ATES system (see Section 2.2).
3. Many of our reservoir-engineering assumptions promote high thermal recovery. For one example, we neglect advective heat loss, which promotes high thermal efficiency (Section 2.4). Furthermore, we assume a reverse faulting regime for the base case (i.e., $\alpha_{II} = 1$), which allows for higher flow rates than would be allowed in normal or strike-slip faulting regimes (see Section 2.2). Finally, we assume a homogeneous reservoir, but heterogeneity would decrease the thermal efficiency [10,15].

We define γ as the ratio of HT-ATES's LCOH to the cost of electricity. Since the MEVT is defined with respect to the cost of electrical resistance heating, the MEVT is the transmissivity that results in $\gamma = 1{:}1$. While the cost of electricity is an assumed value, it is less important than the ratio given by γ because the cost of electricity scales both the operating cost of HT-ATES and the cost of electrical resistance heating.

3. Results

In Section 3.1, we plot the three constraints in terms of COP and flow rate, so that they can be compared visually. In Section 3.2, we present results for the optimal flow rate and well spacing. In Section 3.3, we explore the thermal performance as a function of depth. In Section 3.4, we show the LCOH, the MEVP, and the MEVT. In Section 3.5, we discuss the optimal depth for HT-ATES. Note that we use the optimal flow rate and well spacing throughout Section 3, unless otherwise noted. When results are presented as a function of depth, the depth ranges from 50 m to 2667 m. We choose 2667 m as a cutoff because the geothermal temperature equals the waste heat temperature at this depth.

3.1. The three constraints

All three constraints are illustrated with respect to COP and mass flow rate in Fig. 3. The black curves show COP versus mass flow rate from Eq. (2), with reservoir transmissivity indicated on the plot. The solid black line represents the base case, while the dotted lines have different values of permeability. Higher flow rates imply lower COP because the pumps must perform more work. Constraint I is illustrated by a family of yellow curves, which indicate different reservoir thickness values. Constraint I must be plotted as multiple curves because the reservoir volume depends on the reservoir thickness (Eq. (3)). Constraint II is illustrated by a blue line (Eq. (5)), and Constraint III is represented by a red star for the base case. Note that the base case is a unique scenario chosen so that all three constraints imply the same flow rate. Under these circumstances, the flow rate and well spacing

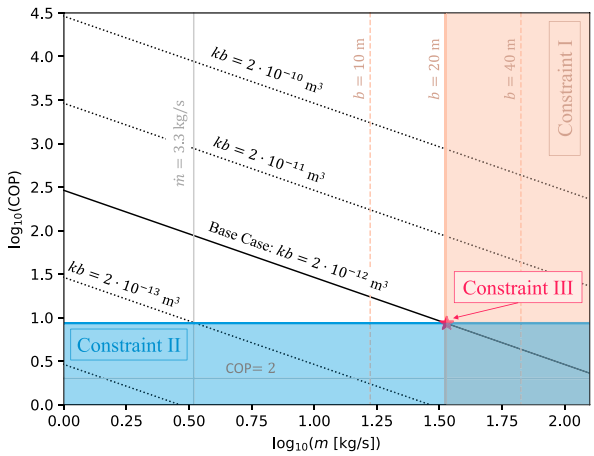

Fig. 3. The logarithm of coefficient of performance (COP) plotted versus the logarithm of mass flow rate with three constraints overlaid. The black curves represent COP versus flow rate. The family of yellow curves represent Constraint I, the blue curve represents Constraint II, and the red star indicates the flow rate that minimizes LCOH from Constraint III (base case). The flow rate and COP must exist outside of the shaded regions from Constraints I and II and to the left of the flow rate implied by Constraint III. Other conditions that are unfavorable, such as COP < 2 or low flow rate (arbitrarily chosen as < 3.3 kg/s) are illustrated in gray. The well spacing is 151 m (which is optimal for the base case), and the depth is 575 m.

from the reservoir constraints are equal to those from the economic constraints. Still, if the reservoir depth, thickness, or permeability were changed, then only two constraints would overlap at the same flow rate.

The COP that leads to HF is independent of the flow rate (which we can see because the blue line is horizontal in Fig. 3), permeability, and reservoir thickness (as indicated by inspection of Eq. (5)). Instead, it depends only on parameters related to the effective stress and the temperature difference. Practically speaking, an engineer can only change the depth or the temperature difference to alter the COP that leads to HF. Inspection of Constraint II highlights that the flow rate that leads to HF may be very low for some reservoir transmissivities. To achieve a flow rate above 3.3 kg/s without HF, the transmissivity must be greater than $2 \cdot 10^{-13}$ m^2 for the base-case depth and stress state. At greater depths, the overburden stress suppresses HF, and the flow rate can be larger, while at shallower depths, the flow rate would need to be less.

The COP = 2 line indicates that the electric work put into pumping is equal to the thermal heat retrieved (i.e., it is equivalent to γ = 1:1 if capital costs are neglected). It is therefore interesting that Constraint II implies a COP that is much larger than 2, which holds for a broad range of parameters in Eq. (5). The COP associated with Constraint II indicates that an HT-ATES will recover more heat than the work that was put into pumping if HF does not occur. Furthermore, even though COP is a measure of thermal recovery efficiency with respect to pumping work, it should not be used to make decisions about the flow rate for HT-ATES. In fact, to maximize the COP, one would select a flow rate approaching zero, which would return essentially no heat. Metrics other than the COP, such as the LCOH (as discussed in Section 3.4), may be more appropriate to make decisions about flow rate. Nevertheless, COP provides a valuable first step to eliminate sites with insufficient permeability.

3.2. Optimal well spacing and flow rate

Fig. 4 plots the flow rate versus the well spacing for each constraint. Constraint I shows that as the well spacing increases, the flow rate increases because a larger reservoir volume can store more heat (Eq. (3)). Constraint II shows that as the well spacing decreases, the flow rate can be increased without leading to HF (Eq. (4)). The maximum flow rate that a reservoir can support (i.e., m_{res}) is found at the intersection between Constraints I and II. Under these conditions, all the heat is effectively stored, and HF does not occur. Note that in the reservoir-constrained regime, the flow rate is more sensitive to well spacing when $L < L^*$ than when $L > L^*$. Constraint III shows that the flow rate that minimizes LCOH increases as well spacing decreases (Eq. (9)). If the curves from Constraints I and III intersect, the well spacing and flow rate come from the economic constraints and should be operated at values lower than the maximum that reservoir can support (i.e., $L^* = L_{econ} \leq L_{res}$ and $m^* = m_{econ} \leq m_{res}$). Fig. 4(a) shows a shallow reservoir in the reservoir-constrained regime. The flow rate is limited to 13 kg/s. The LCOH could hypothetically be decreased with higher flow rates, as shown from the Constraint III curve, but this would lead to HF of the reservoir and therefore cannot be pursued. Fig. 4(b) is the base case. Since it is a special case, all three constraints imply the same flow rate (33 kg/s) and well spacing (151 m). Fig. 4(c), shows a deeper reservoir that operates in the economic-constrained regime at $m^* = m_{econ} = 54$ kg/s and $L^* = L_{econ} = 191$ m.

Optimal well spacing and flow rate increase monotonically with respect to depth, as shown in Figs. 5(a) and (b). The reservoir constraints are relevant at shallow depth, while the economic constraints are relevant at great depth. In the reservoir-constrained regime, the optimal well spacing and flow rate increase rapidly with respect to depth (although the well spacing increases at a decreasing rate). Physically, this is because a greater depth has a greater associated lithostatic stress, which allows both the flow rate and well spacing to increase without leading to HF (Constraint II), while storing all of the injected heat (Constraint I). In the economic-constrained regime, the well spacing and flow rate increase more slowly with respect to depth. Physically, this makes sense because the well spacing and flow rate are both limited below their maximum reservoir-constrained values (i.e., $L_{econ} < L_{res}$ and $m_{econ} < m_{res}$) within the economic-constrained regime. The economic constraints can lead to reductions of up to 64 kg/s and 79 m in the flow rate and well spacing, respectively, compared to the maximum flow rate the reservoir could support at a depth of 2667 m. These reductions are equivalent to 46% for the flow rate and a 25% for the well spacing. The optimal well spacing is always $1.8R_{th}$, regardless of depth.

The optimal well spacing and flow rate also increase monotonically with respect to permeability, as shown in Fig. 5(c). The reservoir constraints are relevant at low permeability, while the economic constraints are relevant at high permeability. For the base-case depth, the transition point from the reservoir-constrained regime to the economic-constrained regime occurs near a permeability of 10^{-13} m^2. This transition point occurs at smaller permeability as the depth increases, which matches physical intuition, because a smaller permeability leads to a larger pressure at the injection well (Eq. (1)), if the flow is held constant. Therefore, the transition happens at a greater depth, where larger lithostatic stress suppresses HF.

It is possible to draw conclusions directly from examining the equations in Section 2. In the reservoir-constrained regime, Eq. (10) shows that the optimal well spacing is independent of the reservoir thickness. Examination of Eqs. (3) and (4) allows us to conclude that the flow rate is directly proportional to the reservoir thickness, in the reservoir-constrained regime. In contrast, in the economic-constrained regime, the well spacing depends on the reservoir thickness, as can be seen in Eq. (11). This dependence leads to a nonlinearity in the flow rate with respect to the reservoir thickness, since the flow rate depends on both the reservoir thickness and the well spacing (see Eqs. (3) and (9)), and the well spacing also depends on the reservoir thickness.

3.3. Thermal performance as a function of depth

The annual amount of heat injected, recovered, and lost to the surrounding rock is shown as a function of depth in Fig. 6(a).

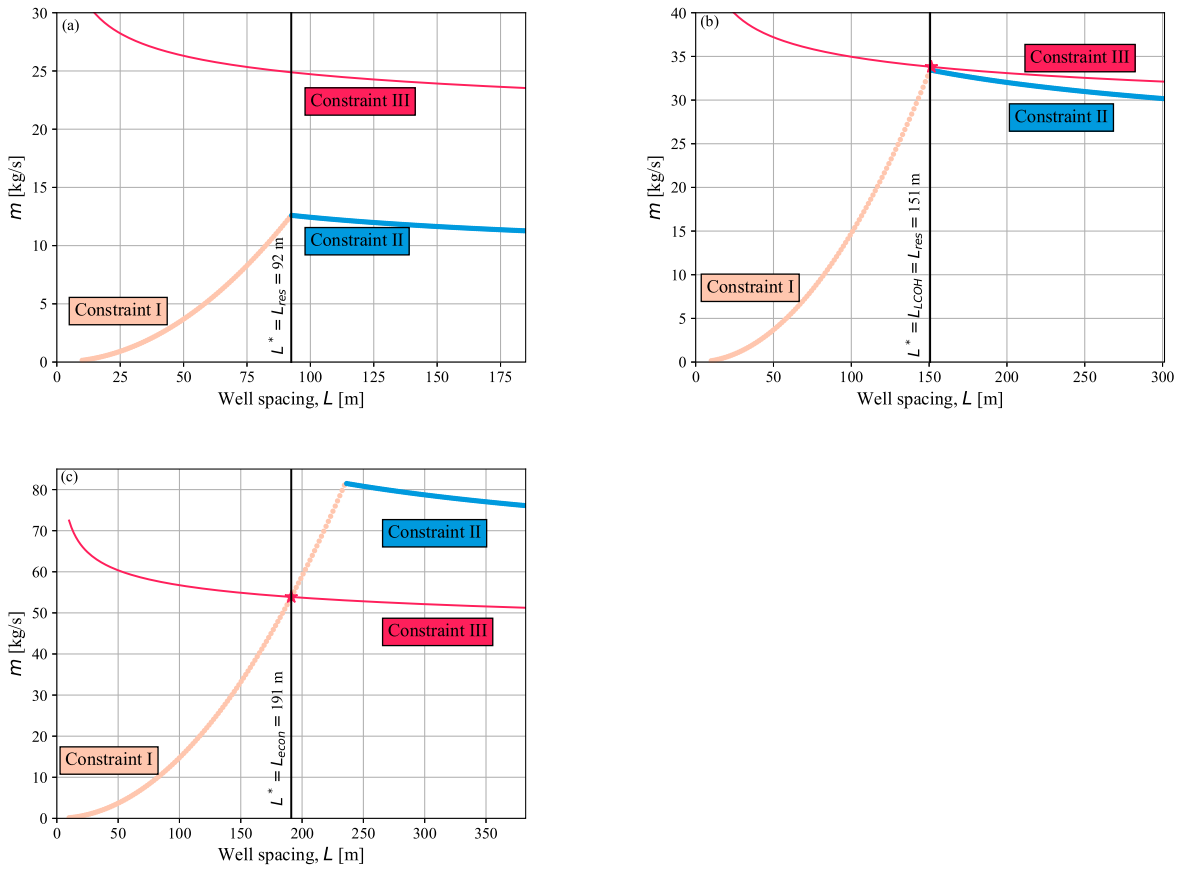

Fig. 4. Plots of mass flow rate versus well spacing to depict the constraints leading to optimal well spacing and flow rate at depths of (a) 200 m, (b) 575 m (base case), and (c) 1500 m. In (a), Constraints I and II (the reservoir-engineering constraints) limit the flow rate and well spacing. In (b), all three constraints are balanced and point to the same flow rate and well spacing. In (c), Constraints I and III (the economic constraints) limit the well spacing and flow rate. The red star shows the point where Constraints I and III intersect, when relevant.

The injected heat is proportional to the optimal flow rate in Fig. 5(b). The injected heat increases rapidly and linearly with respect to depth within the reservoir-constrained regime. This increase continues at a slower (but still linear) rate in the reservoir-constrained regime.

The heat loss displays a non-monotonic relationship with respect to depth, but the thermal efficiency increases monotonically. The heat loss shows non-monotonicity due to trade-offs between: (a) the interfacial area for heat loss (i.e., A in Eq. (13)) and (b) the temperature gradient (which is proportional to $T_{CV} - T_G$ in Eq. (13)). Going from shallow to deep, the heat loss initially increases due to the larger interfacial area. At 850 m deep, the heat loss hits its maximum. Below that depth, the temperature gradient, and therefore the heat loss per area, is small. Therefore, the heat loss decreases with depth, despite more heat injection and larger interfacial area. Even though the heat lost has a non-monotonic relationship with depth, the fraction of heat lost to heat injected decreases monotonically with depth. This trend results in increased thermal efficiency with depth, as shown in Fig. 6(b). The results are presented down to depths of 2667 m, where the geothermal temperature equals the waste-heat temperature, heat losses become zero, and the thermal efficiency is 100%. Trends about heat loss and thermal efficiency can be further understood by examining Eqs. (12) and (13) and examining T_{WH}, T_{CV}, T_G, and T_{DH} in Fig. 6(b).

The heat recovered increases with respect to depth, due to the larger amount of heat injected and the higher thermal efficiency. This increase is approximately linear with respect to depth, with a large slope in the reservoir-constrained regime and a somewhat smaller slope within the economic-constrained regime. For our base case, 13.8 $GW_{th}h$ are injected, and 10.8 $GW_{th}h$ are recovered each year.

3.4. Levelized cost of heat and minimum economically-viable transmissivity

The LCOH is plotted as a function of depth in Fig. 7(a). LCOH is large at shallow depths, hits a minimum at an intermediate depth, and gradually increases at greater depths. For the base-case scenario, LCOH varies by a factor of less than 2.5 with respect to depth, in the range of depths considered. The minimum LCOH is \$0.040/$kW_{th}h$ at 272 m and increases up to >\$0.08/$kW_{th}h$ for depths equal to 50 m and 2667 m. Likewise, the LCOH is fairly insensitive to the faulting regime. The minimum LCOH for $b = 20$ m and $\alpha_{II} = 0.8$ is \$0.048/$kW_{th}h$, which is approximately 20% larger than the base case with $\alpha_{II} = 1.0$.

The LCOH minimum occurs because of a trade-off between the increased thermal performance with depth (as discussed in Section 3.3) and the increased costs with depth. This trade-off is illustrated in Fig. 7(b), which shows equivalent annualized capital cost, annual operating cost, and annual heat recovered. The operating cost is insignificant at shallow depths, but the capital cost is high compared to the heat recovered. As depth increases, LCOH is minimized because the heat recovered becomes large compared to the capital cost, and the operating costs remain small. We denote the depth where LCOH is minimized as d^*_{LCOH}. Since d^*_{LCOH} is a function of reservoir thickness and faulting regime, we discuss it in further detail in Section 3.5. As depth continues to increase, operating cost increases at an increasing rate, which increases the LCOH. Going even deeper (in the economic-constrained regime), the operating cost is equal to the annualized capital cost (see Eq. (8)), and these combined costs are high enough that the LCOH continues to increase, despite recovering more heat as depth increases.

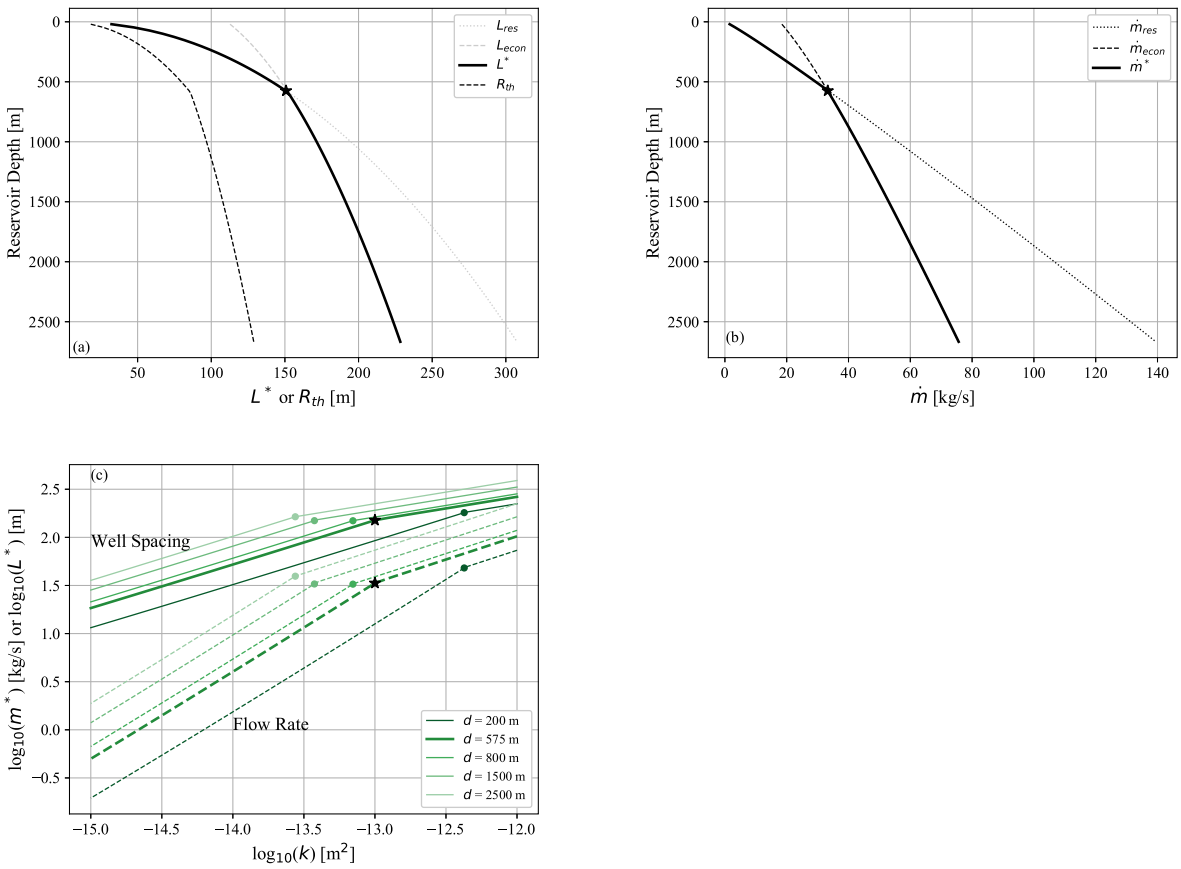

Fig. 5. Optimal well spacing and flow rate. In (a), the depth versus the optimal well spacing and thermal radius are shown. In (b), the depth versus the optimal flow rate is shown. In both (a) and (b), the dashed line indicates the value from the economic constraints, the dotted line indicates the value from the reservoir constraints, and the solid bold line indicates the optimal value, which overlaps the dotted or dashed line, depending on the regime. In (c), the well spacing (solid lines) and flow rate (dashed lines) are plotted versus permeability at different depths. The transition from the reservoir-constrained regime to the economic-constrained regime is marked with a black star for the base case in all three figures; the transition is marked with dots for other depths in (c).

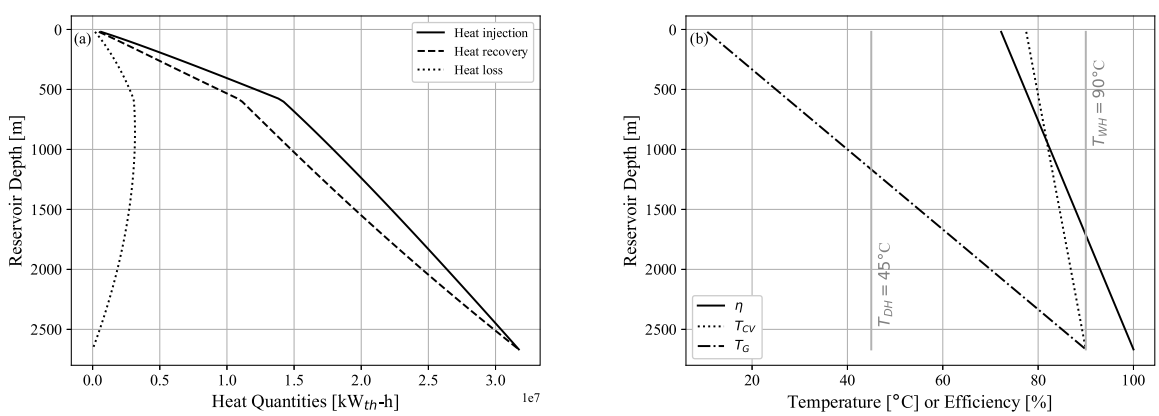

Fig. 6. (a) Annual heat injected, recovered, and lost as a function of depth for a HT-ATES doublet. (b) Thermal efficiency (η), control volume temperature at the end of the storing stage (T_{CV}), and geothermal temperature (T_G) as a function of depth. Also shown in gray are the district heating return temperature (T_{DH}) and the waste heat supply temperature (T_{WH}).

Fig. 8(a) shows the LCOH as a function of permeability for various reservoir thicknesses and faulting regimes (controlled by α_{II}). As permeability decreases, the LCOH increases. At some critical permeability, the LCOH is equal to the cost of electricity. This is the MEVP, k_{min}, as was introduced in Section 2.5. If the permeability falls below k_{min}, heat could certainly be generated with electrical resistance heating for a lower cost than the HT-ATES could provide. The MEVP is marked with a star in Fig. 8(a) and is $k_{min} = 2.8 \cdot 10^{-14}$ m^2 for the base-case scenario.

The MEVP depends on the depth, as shown in Fig. 8(b). The MEVP is minimized at a depth of 465 m for the base case. We denote the depth where the MEVP is minimized as d^*_{kmin}, note that it is a function of reservoir thickness and faulting regime, and discuss in more detail in Section 3.5.

While the MEVP is the permeability that results in a one-to-one ratio of heat to electric cost (i.e., γ =1:1), the analysis can be extended to look for the permeability that would result in lower LCOH and more favorable cost ratios. Fig. 9(a) plots the permeability as a function of

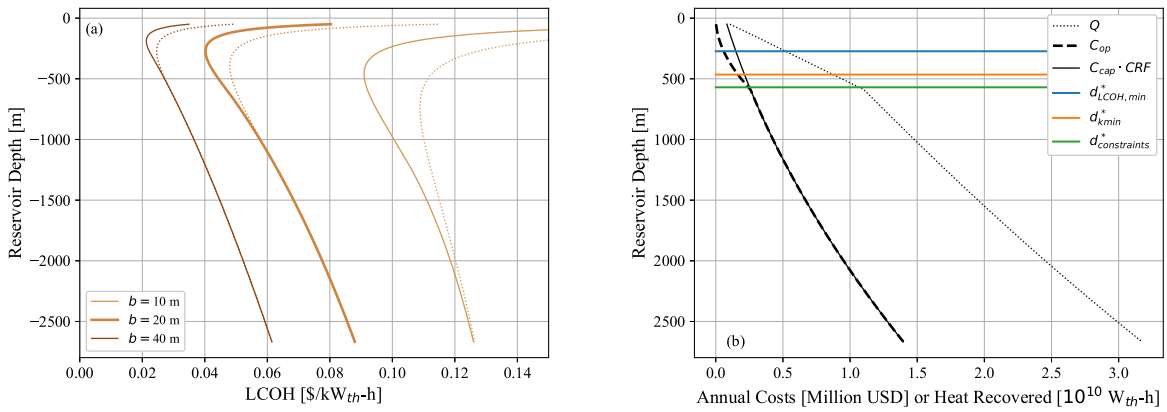

Fig. 7. (a) Depth versus LCOH and (b) depth versus annual operating costs (C_{op}), equivalent annualized capital costs ($C_{cap} \cdot CRF$) and annual heat recovery per doublet (Q), for base-case permeability and reservoir thickness. In (a), the base-case scenario is plotted with a bold line, solid lines use $\alpha_{II} = 1$, dotted lines use $\alpha_{II} = 0.8$ to represent an alternative faulting regime, and color shade corresponds to the reservoir thickness. In (b), various measures of optimal depth are also plotted for reference (see Section 3.5).

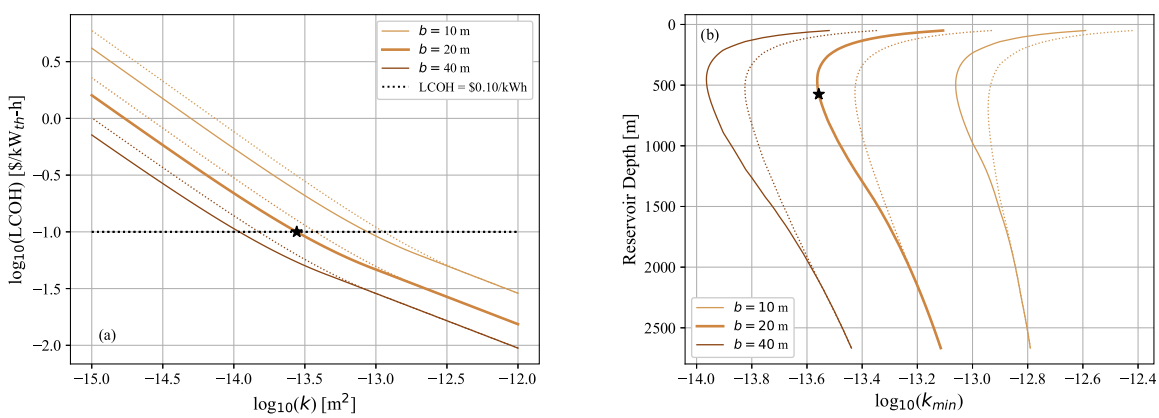

Fig. 8. (a) The logarithm of LCOH as a function of the logarithm of permeability and (b) the reservoir depth versus the logarithm of the MEVP. The bold lines are used to indicate the base-case reservoir thickness, and the MEVP for the base-case reservoir thickness is marked by a star. The solid lines use the base-case faulting regime (i.e., $\alpha_{II} = 1$), dotted lines use the alternative faulting regime (i.e., $\alpha_{II} = 0.8$), and color shade corresponds to aquifer thickness (i.e., b).

reservoir thickness that results in γ equal to 1:1, 1:2, and 1:4. The 1:2 and 1:4 ratios correspond to LCOH of $0.05/kWh$_{th}$ and $0.025/kWh$_{th}$, respectively. The permeability required for γ =1:4 is greater than ten times the permeability required for γ =1:1.

The MEVP decreases as the reservoir thickness increases, suggesting that the transmissivity may be a more important parameter than the permeability. The MEVT is the product of the MEVP and the reservoir thickness, $k_{min}b$, and is plotted versus the reservoir thickness in Fig. 9(b). Over the range of $10 < b < 100$ m, the MEVP varies by a factor of 24, while the MEVT varies by only a factor of 2.4.

Fig. 9(c) shows contours of LCOH as a function of reservoir depth, transmissivity, and faulting regime. The LCOH is most sensitive to the transmissivity, with higher transmissivity associated with lower LCOH. The LCOH is halved and quartered, respectively, by an increase in transmissivity by a factor of three and 12. The LCOH is less sensitive to depth and is minimized at an intermediate depth. For example, at $kb = 10^{-12.25}$ m^3, the optimal depth is at $\approx$ 500 m. Finally, the LCOH is relatively insensitive to the faulting regime, especially at great depths within the economic-constrained regime. This insensitivity is especially true at great depths (i.e., within the economic-constrained regime), where the solid and dashed lines overlap in Fig. 9(c).

The red curve in Fig. 9(c) depicts the MEVT. Like the other contours, it is relatively insensitive to depth and faulting regime. The MEVT varies by less than a factor of three with respect to depth over the range of 50 to 2667 m. Furthermore, the MEVT varies by less than a factor of 1.5 between $\alpha_{II} = 1.0$ and 0.8.

3.5. Measures of optimal depth

In this section, we explore the optimal depth for an HT-ATES reservoir, which has two measures (introduced in Section 3.4): (a) the depth where the LCOH is minimized, d^*_{LCOH}, and (b) the depth where the MEVP is minimized, d^*_{kmin}. These optimal depth values are plotted in Fig. 10, and they range from 189 m to 742 m for the tested parameters (i.e., combinations of b = 10, 20, and 40 m and α_{II} = 1.0 and 0.8). By both measures, the optimal depth becomes shallower as the reservoir becomes thicker. The optimal depth in the alternate faulting regime is deeper than the base-case faulting regime, due to the influence the stress state has on the HF pressure. We also plot the depth where all three constraints are equal, $d_{constraints}$, which indicates where the reservoir-constrained regime transitions to the economic-constrained regime. The depth where LCOH is minimized is shallower than the depth where all three constraints are equal for all the combinations of parameters that we considered, and it is possible that LCOH is always minimized in the reservoir-constrained regime, although we did not exhaustively explore the parameter space.

4. Discussion

4.1. Optimal well spacing and flow rate

The optimal well spacing and flow rate are determined from either the reservoir constraints or the economic constraints, and choosing the correct well spacing and flow rate is essential both technically and

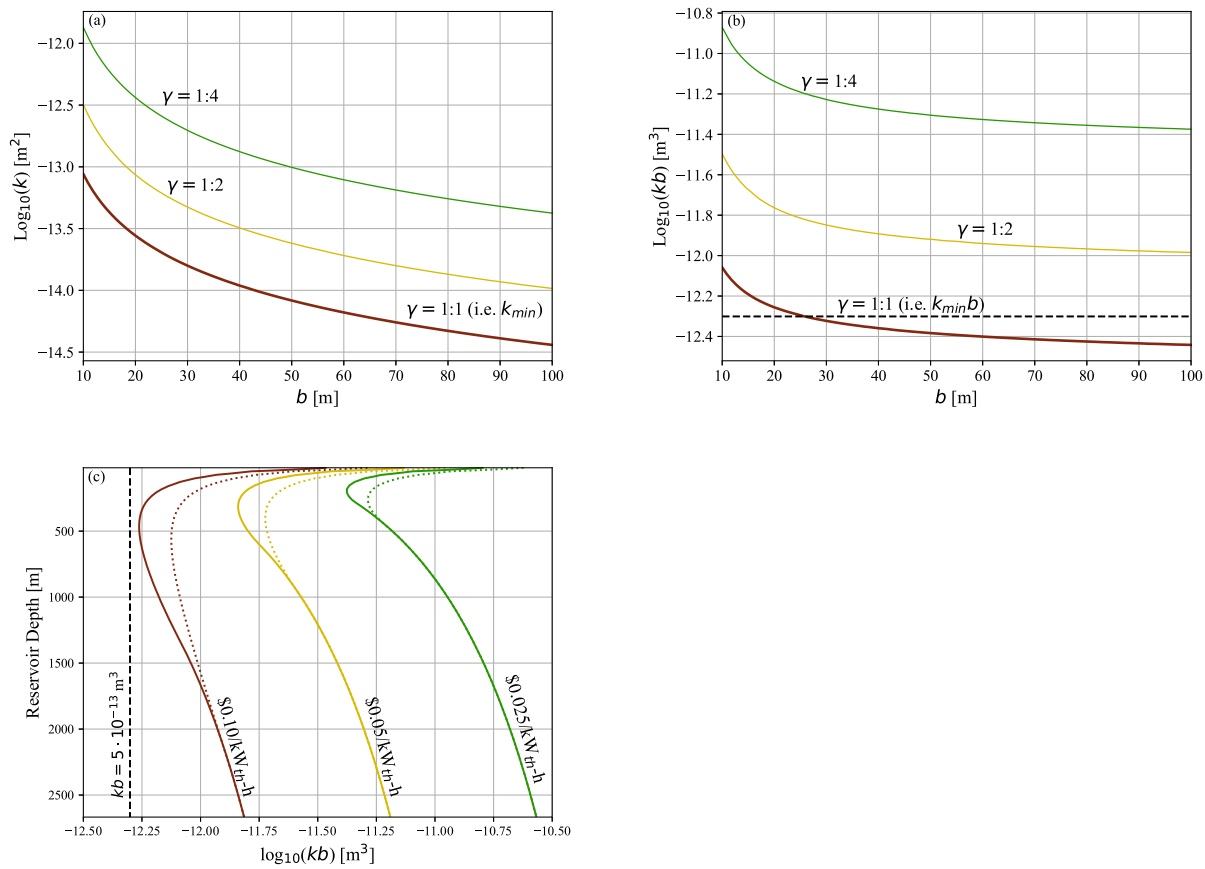

Fig. 9. (a) Logarithm of permeability versus reservoir thickness and (b) logarithm of transmissivity versus reservoir thickness that result in γ equal to 1:1, 1:2, and 1:4. (c) LCOH contours [\$/kWh$_{th}$] in reservoir depth versus logarithm of transmissivity for reservoir thickness equal to 20 m. Curves are colored by γ, the ratio of the LCOH to the electricity cost. Red indicates the cost of heat equals the cost of electricity (\$0.10/kWh) and corresponds to the minimum economically-viable permeability and/or transmissivity, yellow indicates the cost of heat is half the cost of electricity (\$0.05/kWh), and green indicates the cost of heat is one fourth the cost of electricity (\$0.025/kWh). In (a) and (b) the base-case depth is used (575 m). In (b) and (c) the black dashed line shows the proposed global value of MEVT, $5 \cdot 10^{-13}$ m^3. In (c), the dotted lines show the alternative faulting regime (i.e., $\alpha_{II} = 0.8$).

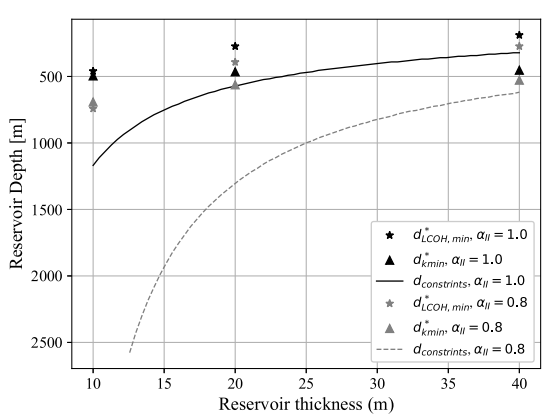

Fig. 10. Measures of optimal depth versus reservoir thickness. The depth of where LCOH is minimized (d^*_{LCOH}) and the depth where the MEVP is minimized (d^*_{kmin}) are plotted as points for reservoir thickness of 10, 20, and 40 m. The depth where all three constraints are equal ($d_{constraints}$) is plotted with a continuous curve. Black indicates a reverse faulting regime ($\alpha_{II} = 1.0$), while gray indicates the alternative faulting regime ($\alpha_{II} = 0.8$).

economically. Suppose an HT-ATES system falls within the reservoir-constrained regime but instead uses the flow rate and well spacing as determined by the economic constraints. In that case, HF is likely to occur, which could enhance the confining units' permeability and lead to loss of heat or contamination of overlying or underlying groundwater. On the other hand, if an HT-ATES system falls within the economic-constrained regime but instead uses the flow rate and well spacing as determined by the reservoir constraints, the operating costs and LCOH would be increased. For example if m_{res} and L_{res} are used instead of m_{econ} and L_{econ} at a depth of 2667 m, the operating costs are increased by 245% and the LCOH is increased by 22%.

The optimal well spacing derived in this paper for HT-ATES does not directly optimize for the thermal efficiency. Instead, the relationship for L^* indirectly accounts for thermal efficiency with Constraint I, which ensures the reservoir can store the heat provided, and Constraint III, which selects the well spacing and flow rate to minimize the LCOH. In contrast to our approach, well spacing recommendations from the LT-ATES literature are usually based, at least partially, on avoiding thermal breakthrough to increase the thermal efficiency [5,7,9]. Despite optimizing for different goals, our value of optimal well spacing, $L^* = 1.8R_{th}$, is within the range (one to more than three thermal radii [5–9]) recommended for LT-ATES systems. This agreement suggests that using a well spacing of $\approx L^* = 1.8R_{th}$ is likely to result in high thermal efficiency, with relatively low amounts of thermal breakthrough, which could be farther assessed with hydro-thermal numerical models.

Even though our value of L^* is within the range for LT-ATES, L^* is at the lower end of the range. While some studies suggest a spacing between hot and cold wells as small as one to two thermal radii [5,8], it seems that more studies advocate spacing of ≥ 2.5 thermal radii [6,7,9]. A tighter spacing for HT-ATES makes some intuitive sense if we think about the differences between LT-ATES and HT-ATES. Namely, since LT-ATES is used for heating and cooling, thermal breakthrough at the cold well leads to a significant decrease in the system's thermal

efficiency during the cooling stage. In contrast, since HT-ATES is only used for heating, it is plausible that thermal breakthrough at the cold well only has a minor impact on the thermal efficiency, leading to a tighter well spacing for HT-ATES.

Finally, our relatively tight well spacing contrasts with the 3.5 thermal radii suggested by Gao et al. [16] for HT-ATES, which could be explained by different assumptions about heat loss or NRGF. For one thing, our model neglects advective heat loss, which is an acceptable assumption for low-permeability reservoirs, but becomes inaccurate for some of the higher permeabilities that Gao et al. [16] explore. Furthermore, Gao et al. [16] locate the hot well downstream of the cold well, which encourages water from the cold well to reach the hot well earlier, whereas our THM$ approach assumes negligible NRGF.

4.2. Crowding of the subsurface

The subsurface is becoming increasingly crowded, especially near cities, and HT-ATES may help to relieve this congestion by filling a unique role at intermediate depths. Heating applications may be particularly prone to crowding because they need to be located near the end-user to reduce distribution costs and heat loss. LT-ATES systems have congested the shallow subsurface under some European cities [7,9]. Furthermore, direct-use geothermal needs to take place sufficiently deep that there is a high geothermal temperature, and van Wees et al. [22] found an optimum depth of around 1.6 km. Therefore it is encouraging we found that HT-ATES seems to be technically and economically optimal at intermediate depths from 187–726 m (Section 3.5), where competition with shallow (ground source heat pumps and LT-ATES) and deep (direct-use geothermal) heating applications could be minimal. Furthermore, it is economically feasible to target greater depths than 726 m, since the LCOH is relatively insensitive to depth going somewhat deeper (Section 3.4). Therefore, HT-ATES at intermediate depths (and sometimes great depths) could supplement LT-ATES and relieve areas where the shallow subsurface is congested.

4.3. Practical considerations

Our results hint at some practical design considerations for HT-ATES systems.

1. There can be considerable uncertainty in the subsurface properties, which leads to uncertainty in L^*. Therefore, when operating in the reservoir-constrained regime, it may be prudent to design HT-ATES doublets with well spacing that is slightly larger than L^*, because the flow rate decreases at a greater rate when $L < L^*$ than when $L > L^*$ (Fig. 5(a), Section 3.2).
2. Accurate knowledge of the stress state and faulting regime is important for shallow or low-permeability reservoirs in the reservoir-constrained regime, because operating conditions occur near the HF threshold. However, this becomes less important for deep or high-permeability reservoirs, in the economic-constrained regime. The stress state is less important in the economic-constrained regime because the injection pressure is not meant to approach the HF threshold. The diminished importance can be seen in the convergence of the solid and dashed curves in Figs. 7(a), 8(b) and 9(c). Assessments for reservoirs in the economic-constrained regime may be able to save effort and money with somewhat less-rigorous stress characterization than reservoirs in the reservoir-constrained regime would need.
3. Even though a deeper doublet produces more heat (Fig. 7), it is better economically to have multiple doublets at an optimal depth, than one at a greater depth. This way, LCOH is minimized, and the heat demand can be scaled based on the number of doublets installed.

4.4. Minimum economically-viable transmissivity

The MEVT can be approximated as a single value of $k_{min}b = 5 \cdot 10^{-13}$ m^3, as depicted in the dashed black lines in Fig. 9(b) and (c). This is possible because the MEVT is not very sensitive to reservoir thickness, depth, or faulting regime in the range of $10 \leq b \leq 100$ m, $200 \leq d \leq 1500$ m, and $0.8 \leq \alpha_{II} \leq 1.0$. The MEVT is smaller than transmissivity values typically recommended for LT-ATES [11,12] and direct-use geothermal [22] and is also smaller than the value employed in many HT-ATES numerical modeling studies [4,14,17]. This difference could be due to our generous assumptions to find the lowest-possible transmissivity, particularly the assumption that heat has the same cost as electricity (i.e., $\gamma = 1{:}1$). On the other hand, when comparing HT-ATES to LT-ATES, the fluid's energy density is higher, so it may be economically feasible to use reservoirs with lower transmissivity (and therefore lower flow rates) than are traditionally recommended for LT-ATES. Constructing an HT-ATES system in a reservoir with the MEVT would probably result in higher heat prices than could be provided by a natural gas boiler (e.g., see [4]). Therefore transmissivity $> 5 \cdot 10^{-13}$ m^3 would be preferable. Finally, if a reservoir has a transmissivity below the MEVT, it may be possible to enhance the transmissivity using techniques such as radial jet drilling or HF. However, these technologies are untested in conjunction with ATES, to our knowledge, and they will add heterogeneity to the reservoir, which reduces the thermal efficiency [10,15]. Therefore, we believe that the MEVT is a good metric for HT-ATES (in)feasibility.

The MEVT can be used in a pre-assessment of HT-ATES potential, either to rule out unfavorable reservoirs for a particular site or to put an upper bound on HT-ATES capacity at a national or global scale. For a local project, the MEVT can be used to quickly and easily pre-assess many potential reservoirs. If any reservoir's transmissivity falls below the MEVT, it can be removed from consideration. At a regional or global scale, a GIS-based approach could be used to assess the potential of HT-ATES. This approach would first involve finding the reservoirs that (a) have transmissivity above the MEVT and (b) are within the depth range that is feasible for HT-ATES (e.g., from 100–2500 m). The capacity of these reservoirs would represent an upper bound on the potential of HT-ATES. This global HT-ATES potential could be further refined by incorporating other considerations, such as proximity to excess heat supply (e.g., factories, waste incineration, or CHP plants), proximity to heat demand (e.g., cities with DHNs, greenhouses, or large office or industrial buildings), and local climate [27,28]. It may be possible to expand this approach to calculate a cost curve for HT-ATES since our THM$ framework provides the LCOH as a function of depth and transmissivity. This cost curve could be used in energy system modeling to assess future strategies of energy production, use, and storage. The global potential to store heat via HT-ATES has not been assessed to our knowledge. But it could be large in comparison to LT-ATES because (a) HT-ATES is possible over a wide range of depths, and (b) HT-ATES has a higher energy density than LT-ATES. Therefore, a global assessment of HT-ATES is an important research goal.

4.5. Limitations and future work

The analysis presented in this paper relies on several assumptions and therefore has limitations. The assumptions were chosen: (a) to construct an analytical model that clarifies aspects of optimal well spacing, flow rate, and reservoir depth and (b) to be "conservative" in the sense of calculating a MEVT that does not unduly eliminate reservoirs that could be used for HT-ATES. We focused on technical and economic aspects of HT-ATES in a climate where waste heat is available in the summer, and heat is demanded in the winter. We did not consider the regulatory aspects of ATES. We also did not consider alternative climate conditions, which may require heating and cooling or only cooling. The LCOH values reported in this paper are primarily presented to evaluate Constraint III and to calculate the MEVT. The LCOH values should

be interpreted as a first-order estimate, and more robust estimates of LCOH would require techno-economic studies that consider geological, engineering, and economic aspects (e.g., [29]). In our assumptions, we ignored the complexity of reservoir heterogeneity [10]; advective heat loss due to NRGF or thermally-induced buoyancy [15,17,30]; chemical scaling, dissolution, precipitation, and corrosion; clay swelling; well-screen clogging from fine-grained particles [31]; and thermo-poro-elastic deformation [18], which could reduce thermal efficiency and/or damage infrastructure. Our heat loss equation considers conduction from the reservoir to the overlying and underlying units. This heat loss equation represents a reasonable approach when the permeability and the reservoir thickness are small. But this conduction-only approximation becomes less accurate: (a) as reservoir thickness becomes larger and significant amounts of heat is lost laterally via conduction or (b) as permeability becomes larger ($\geq 5 \cdot 10^{-13}$ m^2 [14,15,17,30]) and (buoyant) advective heat loss becomes relevant. Therefore, the reported LCOH for large transmissivity has more uncertainty than for low transmissivity. A robust combination of site characterization, geological modeling, energy-systems scenario modeling, and reservoir modeling is required to comprehensively evaluate the technical, economic, and market potential of HT-ATES at a particular site [32].

Despite the assumptions and limitations mentioned in the previous paragraph, our analysis is valuable for reservoir pre-assessment and understanding the design trade-offs related to well spacing, flow rate, and reservoir depth. The THM$ methodology uses analytical solutions, which allows us to assess reservoir-engineering and economic constraints and leads to: (a) low computational cost and (b) first-order understanding that can be easily gleaned from inspecting the equations. In contrast, assessing THM$ constraints using fully-coupled numerical models would be exceedingly computationally expensive and has some risk of becoming a "black box" with results that are difficult to interpret.

We recommend the following future work, both within and outside the THM$ framework:

1. Our THM$ framework is published as an open-source contribution and can be used to elucidate additional research questions. For example, it would be straightforward to alter parameters like the well radius or specify a depth-dependent permeability within the framework. Furthermore, the THM$ framework could be expanded to consider other aspects of HT-ATES, such as: (a) heat and pressure losses within the wellbore, or (b) more complex models of the heat exchanger and the DHN.
2. As discussed somewhat in Section 4.1, it would be useful to investigate our recommendations for optimal well spacing and flow rate using a hydro-thermal numerical model. We believe that the tight well spacing that we suggest ($L^* = 1.8R_{th}$) is likely appropriate for low-permeability units, which have small amounts of NRGF and advective heat loss. On the other hand, for systems with high permeability and lots of NRGF, a larger well spacing could be more favorable [16]. A thermo-hydro numerical model can elucidate the conditions under which each of these recommendations is appropriate.
3. Data on HT-ATES costs is rare, but uncertainty in LCOH calculations can be reduced with better data, particularly for capital and maintenance costs. Capital and maintenance cost data should be collected and shared.
4. As discussed in Section 4.4, national or global assessments of HT-ATES should be conducted, and cost curves for energy system models should be constructed. This task would rely on huge amounts of transmissivity data, reflecting a land area the size of a country over a wide range of depths (e.g., 100–2500 m). Locating this data and collecting it into one database would be a sizable challenge. Still, the benefits of such an assessment could facilitate intelligent investments in sustainable infrastructure for many decades, or possibly centuries, to come.

5. Conclusions

In this paper, we developed a THM$ analytical approach to balance three constraints on HT-ATES operations. While numerical simulations are useful for gaining insights into HT-ATES, our analytical approach is advantageous. Firstly, it has much lower computational costs. Secondly, physical insights can be gleaned directly from inspecting the equations in Section 2 (i.e., there is little risk of our approach becoming a "black box"). Using this approach, we arrived at several practical conclusions that are useful for the design and pre-assessment of HT-ATES systems:

1. *By balancing the three constraints, we find an optimal well spacing and flow rate (see Sections 2.3 and 3.2).* The well spacing and flow rate are linked, and they are chosen so that the flow rate is maximized without violating any of the three constraints. The reservoir-constrained regime applies to shallow or low-permeability reservoirs (i.e., Constraints I and II). In contrast, deep or high-permeability reservoirs are dictated by the economic-constrained regime (Constraints I and III). In the reservoir-constrained regime, increased flow rate would HF the reservoir, whereas in the economic-constrained regime, increased flow rate would lead to higher LCOH.
2. *The optimal well spacing is $1.8R_{th}$, which is at the lower end of the range suggested for LT-ATES.* This tight spacing makes intuitive sense because thermal breakthrough at the cold well is probably not as bad for the thermal efficiency of HT-ATES as it is for LT-ATES, since HT-ATES is only used for heating whereas LT-ATES is also used for cooling. Nevertheless, there is room to further explore optimal well spacing with hydro-thermal numerical models.
3. *The LCOH is minimized at an intermediate depth.* This minimum occurs because of trade-offs between the amount of heat recovered and the costs, which increase at different rates with respect to depth (see Fig. 7). At shallow depths, the LCOH is large because the capital costs are high with respect to the low amount of heat recovery. At intermediate depths, the LCOH is low because the heat recovery is large, while the capital costs are moderate and the operating costs are low. At great depths, the LCOH is large despite a high amount of heat recovery, because the combined capital and operating costs increase at an increasing rate with depth.
4. *The LCOH of a system is more sensitive to reservoir transmissivity than depth or faulting regime.* We found that the LCOH can vary by orders of magnitude within the range of transmissivities tested (see Fig. 8(a)), whereas it varies by a factor of < 2.5 due to depth and $\approx$1.2 due to the faulting regime (see Fig. 7(a)). The sensitivity of LCOH to transmissivity is considerable because of the wide range (i.e., many orders of magnitude) over which transmissivity varies in nature. Therefore, transmissivity is a key property in determining the economic success of HT-ATES.
5. *Some reservoir transmissivities are so small that it becomes impossible to pump meaningful flow rates without HF.* For the base-case depth and stress state, the flow rate is limited to ≤ 3.3 kg/s, if the transmissivity is $\leq 2 \cdot 10^{-13}$ m^3 (see Fig. 3(a)).
6. *The minimum economically-viable transmissivity (MEVT) can be approximated as a single value of* $5 \cdot 10^{-13}$ m^3. This approximation is possible because the MEVT is relatively insensitive to depth, reservoir thickness, and faulting regime (Fig. 9). The MEVT is perhaps the most useful result of our analysis because it can be used in a pre-assessment at a specific site, or to assess national or global potential for HT-ATES.

CRediT authorship contribution statement

Daniel T. Birdsell: Conceptualization, Methodology, Software, Validation, Visualization, Writing - original draft. **Benjamin M. Adams:** Conceptualization, Methodology, Writing - review & editing. **Martin O. Saar:** Funding acquisition, Writing - review & editing.

Declaration of competing interest

The authors declare that they have no known competing financial interests or personal relationships that could have appeared to influence the work reported in this paper.

Acknowledgments

We would like to thank our colleagues Dr. Anozie Ebigbo, Dr. Alexandros Daniilidis, and Dr. Jonathan Ogland-Hand for insightful discussions that helped with the framing of this paper. We also thank two anonymous reviewers for their comments, which helped to improve the paper.

Funding

This work was supported by HEATSTORE (170153-4401), ELEGANCY, and Innosuisse, Switzerland (Grant number 28305.1 PFIW-IW). HEATSTORE has been subsidized through the ERANET cofund GEOTHERMICA (Project n. 731117), from the European Commission, RVO (the Netherlands), DETEC (Switzerland), FZJ-PtJ (Germany), ADEME (France), EUDP (Denmark), Rannis (Iceland), VEA (Belgium), FRCT (Portugal), and MINECO (Spain). ACT ELEGANCY, Project No 271498, has received funding from DETEC (CH), FZJ/PtJ (DE), RVO (NL), Gassnova (NO), BEIS (UK), Gassco AS and Statoil Petroleum AS, and is cofounded by the European Commission under the Horizon 2020 programme, ACT Grant Agreement No 691712. The Geothermal Energy and Geofluids (GEG.ethz.ch) group also gratefully acknowledges support by the Werner Siemens-Stiftung (Foundation), which also enabled this work.

References

[1] Fleuchaus P, Godschalk B, Stober I, Blum P. Worldwide application of aquifer thermal energy storage–A review. Renew. Sustain. Energy Rev. 2018;94:861–76. http://dx.doi.org/10.1016/j.rser.2018.06.057.

[2] Lee KS. Underground thermal energy storage. London: Springer London; 2013, p. 1–13. http://dx.doi.org/10.1007/978-1-4471-4273-7_2.

[3] Renaldi R, Kiprakis A, Friedrich D. An optimisation framework for thermal energy storage integration in a residential heat pump heating system. Appl. Energy 2017;186:520–9.

[4] Wesselink M, Liu W, Koornneef J, Van Den Broek M. Conceptual market potential framework of high temperature aquifer thermal energy storage-A case study in the Netherlands. Energy 2018;147:477–89. http://dx.doi.org/10.1016/j.energy.2018.01.072.

[5] Kim J, Lee Y, Yoon WS, Jeon JS, Koo M-H, Keehm Y. Numerical modeling of aquifer thermal energy storage system. Energy 2010;35(12):4955–65. http://dx.doi.org/10.1016/j.energy.2010.08.029.

[6] NVOE. Werkwijzen en richtlijnen ondergrondse energieopslag (Methods and guidelines underground energy storage) Nederlandse vereniging voor ondergrondse energieopslag (Dutch society for subsurface energy storage); 2006.

[7] Sommer W, Valstar J, Leusbrock I, Grotenhuis T, Rijnaarts H. Optimization and spatial pattern of large-scale aquifer thermal energy storage. Appl. Energy 2015;137:322–37. http://dx.doi.org/10.1016/j.apenergy.2014.10.019.

[8] Bloemendal M, Olsthoorn T, Boons F. How to achieve optimal and sustainable use of the subsurface for aquifer thermal energy storage. Energy Policy 2014;66:104–14. http://dx.doi.org/10.1016/j.enpol.2013.11.034.

[9] Bloemendal M, Jaxa-Rozen M, Olsthoorn T. Methods for planning of ATES systems. Appl. Energy 2018;216:534–57. http://dx.doi.org/10.1016/j.apenergy.2018.02.068.

[10] Sommer W, Valstar J, van Gaans P, Grotenhuis T, Rijnaarts H. The impact of aquifer heterogeneity on the performance of aquifer thermal energy storage. Water Resour. Res. 2013;49(12):8128–38. http://dx.doi.org/10.1002/2013WR013677.

[11] Snijders A, Drijver B. Open-loop heat pump and thermal energy storage systems. In: Advances in ground-source heat pump systems. Elsevier; 2016, p. 247–68. http://dx.doi.org/10.1016/B978-0-08-100311-4.00009-1.

[12] Schmidt T, Mangold D, Müller-Steinhagen H. Seasonal thermal energy storage in Germany. In: ISES solar world congress. vol. 14. Göteborg, Schweden: 2003. p. 1–7.

[13] Holstenkamp L, Meisel M, Neidig P, Opel O, Steffahn J, Strodel N, et al. Interdisciplinary review of medium-deep aquifer thermal energy storage in North Germany. Energy Procedia 2017;135:327–36. http://dx.doi.org/10.1016/j.egypro.2017.09.524.

[14] Collignon M, Klemetsdal ØS, Møyner O, Alcanié M, Rinaldi AP, Nilsen H, et al. Evaluating thermal losses and storage capacity in high-temperature aquifer thermal energy storage (HT-ATES) systems with well operating limits: Insights from a study-case in the Greater Geneva Basin, Switzerland. Geothermics 2020;85:101773. http://dx.doi.org/10.1016/j.geothermics.2019.101773.

[15] Résonance. Étude du comportement thermo-hydraulique d'un système HT-ATES en aquifère profond. Tech. rep. TR-6001.031/NL, SIG (Services Industriels de Genève); 2017.

[16] Gao L, Zhao J, An Q, Liu X, Du Y. Thermal performance of medium-to-high-temperature aquifer thermal energy storage systems. Appl. Therm. Eng. 2019;146:898–909. http://dx.doi.org/10.1016/j.applthermaleng.2018.09.104.

[17] Mindel JE, Driesner T. HEATSTORE: Preliminary design of a high temperature aquifer thermal energy storage (HT-ATES) system in Geneva based on TH simulations. In: World geothermal congress. Reykjavik, Iceland: 2020. p. 1–12. http://dx.doi.org/10.3929/ethz-b-000444531, Originally accepted at WGC 2020, which was poned to 2021.

[18] Birdsell DT, Saar MO. Modeling ground surface deformation at the Swiss HEATSTORE underground thermal energy storage sites. In: World geothermal congress. Reykjavik, Iceland: ETH Zurich, Institute of Geophysics; 2020, p. 1–6. http://dx.doi.org/10.3929/ethz-b-000421353, Originally accepted at WGC 2020, which was postponed to 2021.

[19] Birdsell DT. Thermo-hydro-mechanical-economic (THM$) code for HT-ATES. 2020, http://dx.doi.org/10.5281/zenodo.4075425, Zenodo.org.

[20] Schaetzle WJ, Brett CE, Grubbs DM, Seppanen MS. Thermal energy storage in aquifers: design and applications. New York: Pergamon Press, Inc.; 1980, Ch. 3.

[21] Yeo IW, Lee K-K. Analytical solution for arbitrarily located multiwells in an anisotropic homogeneous confined aquifer. Water Resour Res 2003;39(5).

[22] van Wees J-D, Kronimus A, Van Putten M, Pluymaekers M, Mijnlieff H, Van Hooff P, et al. Geothermal aquifer performance assessment for direct heat production–Methodology and application to rotliegend aquifers. Neth. J. Geosci. 2012;91(4):651–65. http://dx.doi.org/10.1017/S0016774600000433.

[23] Zoback MD. Reservoir geomechanics. United Kingdom: Cambridge University Press; 2010, http://dx.doi.org/10.1017/CBO9780511586477.

[24] Mines GL. GETEM User Manual. Tech. rep. INL/EXT-16-38751, Idaho National Laboratory; 2016.

[25] Lund H, Østergaard PA, Chang M, Werner S, Svendsen S, Sorknæs P, et al. The status of 4th generation district heating: Research and results. Energy 2018;164:147–59. http://dx.doi.org/10.1016/j.energy.2018.08.206.

[26] Lund H, Werner S, Wiltshire R, Svendsen S, Thorsen JE, Hvelplund F, et al. 4th generation district heating (4GDH): Integrating smart thermal grids into future sustainable energy systems. Energy 2014;68:1–11. http://dx.doi.org/10.1016/j.energy.2014.02.089.

[27] Lu H, Tian P, Guan Y, Yu S. Integrated suitability, vulnerability and sustainability indicators for assessing the global potential of aquifer thermal energy storage. Appl. Energy 2019;239:747–56. http://dx.doi.org/10.1016/j.apenergy.2019.01.144.

[28] Bloemendal M, Olsthoorn T, van de Ven F. Combining climatic and geo-hydrological preconditions as a method to determine world potential for aquifer thermal energy storage. Sci. Total Environ. 2015;538:621–33. http://dx.doi.org/10.1016/j.scitotenv.2015.07.084.

[29] Daniilidis A, Alpsoy B, Herber R. Impact of technical and economic uncertainties on the economic performance of a deep geothermal heat system. Renew. Energy 2017;114:805–16. http://dx.doi.org/10.1016/j.renene.2017.07.090.

[30] Molz F, Melville J, Parr AD, King D, Hopf M. Aquifer thermal energy storage: A well doublet experiment at increased temperatures. Water Resour. Res. 1983;19(1):149–60.

[31] Jenne E, Andersson O, Willemsen A. Well, hydrology, and geochemistry problems encountered in ATES systems and their solutions. Tech. rep. 929153, SAE Technical Paper; 1992.

[32] Guglielmetti L, et al. HEATSTORE SWITZERLAND: New opportunities of geothermal district heating network sustainable growth by high temperature aquifer thermal energy storage development. In: World geothermal congress. Reykjavik, Iceland.: University of Geneva; 2020, p. 1–13, Originally accepted at WGC 2020, which was postponed to 2021; https://archive-ouverte.unige.ch/unige:136509.